JOURNAL OF AIRCRAFT
Vol. 32, No. 5, September–October 1995

Effect of Blade-Tip Planform on Shock Wave of Advancing Helicopter Blade

Takashi Aoyama*
National Aerospace Laboratory, Tokyo 182, Japan
Keiji Kawachi†
University of Tokyo, Tokyo 153, Japan
and
Shigeru Saito‡
National Aerospace Laboratory, Tokyo 181, Japan

The effect of blade-tip planform on the behavior of shock waves on the advancing rotor blade was investigated in detail using a calculation method that solves three-dimensional Euler equations by an implicit finite difference method. The Newton iterative method was applied to obtain the unsteady solution in forward flight. The calculations were performed for the blades having the NACA 0012 airfoil section along the entire blade span to investigate the planform effect alone. The parametric study clarified the effect of the sweep and the taper on shock-wave generation. In addition, a guideline of the blade planform design for the advancing blade was suggested, and a newly devised tip planform that prevents shock-wave generation was proposed.

Nomenclature

AR	=	aspect ratio
C	=	chord length
C_p	=	pressure coefficient
M_n	=	incident unsteady Mach number, $M_\infty \sin \psi + M_T(r/R)$
M_T	=	Mach number based on rotating tip speed
M_∞	=	freestream Mach number
R	=	rotor radius
r	=	radial station
x/C	=	chordwise distance nondimensionalized by chord length
x, y, z	=	components of rotating Cartesian coordinate system fixed with blade
$\Delta(-C_p)$	=	defined in Fig. 3
ξ, η, ζ	=	arbitrary curvilinear coordinate system
μ	=	advance ratio
ψ	=	azimuth angle

Introduction

SHOCK waves are generated on the advancing side and stall on the retreating side of the blade tip of a helicopter rotor in forward flight condition. These phenomena cause an increase in drag, vibration, and noise. It is known that modification of the blade-tip planform may limit shock-wave generation and stall occurrence. Many efforts have been made in both experimental and theoretical researches about the blade-tip planform in the forward flight condition.

The experimental studies were focused on only a few tip planforms. The detailed characteristics of each individual blade tip have been obtained through the studies, but the comprehensive characteristics of blade-tip planforms are still not well understood. The theoretical approach using the computational fluid dynamics (CFD) technique has the advantage of obtaining more easily the comprehensive characteristics of blade-tip planforms as well as the detailed flowfield around the blade tips. The calculations, however, have been limited for the advancing side alone because the present levels of computer processing power, memory, and the CFD technique are limited. Theoretical research regarding the blade-tip planform on the advancing side was made by solving the transonic small disturbance (TSD) equation[1,2] or full-potential equation[3,4] in the early stage, where only a few tip planforms were calculated. These equations are not suitable for the calculation in the strong shock-wave condition. Then, Euler equations were solved,[5] but the results were very limited. Navier–Stokes equations[6,7] were solved recently, but the calculations were done only for the steady hovering condition instead of the unsteady forward flight condition.

In this study, various tip planforms are calculated comprehensively and the effect of the blade-tip planform on the unsteady behavior of the shock wave on the advancing blade is investigated in detail using the calculation method that solves Euler equations by a time-accurate method and a higher-order upwind scheme. A guideline of a blade planform design for the advancing side is suggested and a newly devised tip planform that prevents shock-wave generation is proposed.

Calculation Method

A brief explanation of the present calculation method is as follows. The detailed calculation method was given in a previous paper.[8] The governing equations are the three-dimensional unsteady Euler equations in the rotating Cartesian coordinate system fixed with the blade. The numerical method to solve the governing equations is an implicit finite difference scheme. A higher-order upwind scheme based on TVD is applied for the inviscid terms of the explicit right-hand side. To obtain the unsteady solution in the forward flight condition of a helicopter rotor, the Newton iterative method is added. In the beginning of the calculation, the steady calculation is conducted at $\psi = 90$ deg, using the implicit time-marching method. Then, the unsteady calculation is started from this initial condition. Periodic converged solutions of chordwise pressure distributions are obtained at $\psi = 200$ deg, and these

Received April 29, 1994; revision received Dec. 21, 1994; accepted for publication Feb. 20, 1995. Copyright © 1995 by the American Institute of Aeronautics and Astronautics, Inc. All rights reserved.

*Researcher, Computational Sciences Division, 7-44-1, Jindaiji-Higashi, Chofu. Member AIAA.
†Professor, Research Center for Advanced Science and Technology, 4-6-1, Komaba, Meguro-ku. Member AIAA.
‡Head of Flight Test Laboratory, Flight Research Division, 6-13-1, Osawa, Mitaka. Member AIAA.

converged solutions are presented in this article at each azimuth angle. Four iterations are sufficient to reduce the residual at each time step. The typical dividing number along the azimuthal direction is about 1000/rev.

To simplify the calculation, an algebraic method is adopted for the grid generation. The grid is C-H type and it consists of 105 × 41 × 27 points, which was determined by a preliminary grid sensitivity study. The 75 × 19 points are distributed on the blade surface and orthogonalized. All the boundary conditions are explicitly specified to simplify the calculation. Surface tangency and adiabatic conditions are applied on the blade surface. All the quantities, density, velocities, and energy, are set to the freestream values at the far-field boundary and the outer boundary of the ζ axis. The direction of the freestream velocity observed from the blade-fixed coordinate system changes at every moment in the forward flight condition. All the quantities are extrapolated from the interior at the inner boundary of the ζ axis. The pressure is set to the freestream value at the outflow boundary. The grid has cuts and the flow properties are averaged between above and below along these cuts.

The pressure distributions on the blade surface calculated by the present method are compared with experimental data to validate the capability of the present method. Figures 1a and 1b show a comparison of calculated and experimental results[9] of surface pressure distributions on a model helicopter rotor in forward flight. The comparisons are done in nonlifting conditions because the effective angle of attack is ordinarily small on the advancing side of a helicopter rotor in forward flight conditions. The model rotor has two untwisted blades. The AR of the blade is 7 and the airfoil section is NACA 0012. The calculated results are in good agreement with the experimental data at every azimuth position for the two cases shown in Figs. 1a and 1b. The shock wave keeps its strength after passing through the azimuth position of $\psi = 90$ deg, where the inflow velocity is maximum at every radial station. The calculated results capture well this unsteady shock-wave behavior.

Behavior of the Shock Wave on a Rectangular Blade

Spanwise and Azimuthwise Variation

The behavior of the shock wave on a rectangular blade is analyzed as a baseline. The blade is the same one described previously. Figure 2 shows the calculated result of the Mach contours on the blade surface. Variation of the shock-wave region can be observed in this figure. The pressure jump $\Delta(-C_p)$, defined in Fig. 3, which is generated by the shock wave, is introduced as an index to express the variation of the shock-wave strength in detail.

Effect of Unsteadiness

To investigate the effect of unsteadiness of the blade operating condition on the spanwise variations of $\Delta(-C_p)$, the following three cases are compared: 1) $M_\infty = 0.31$, $M_T = 0.6$, $\mu \approx 0.52$; 2) $M_\infty = 0.21$, $M_T = 0.7$, $\mu = 0.3$; and 3) $M_\infty = 0.11$, $M_T = 0.8$, $\mu \approx 0.14$. All three cases give the same tip Mach number, 0.91, at $\psi = 90$ deg, and both the rotational speed and the forward speed were varied among the cases. Case (1) is the most unsteady condition because the variation of the relative airspeed toward a blade increases as the advance ratio becomes larger. The calculated results presented in Fig. 4 show that the timewise variation of $\Delta(-C_p)$ becomes more remarkable as the advance ratio increases. In addition, comparison of the three cases at $\psi = 90$ deg shows that the shock wave becomes stronger as the advance ratio increases. This is because M_n becomes larger as the advance ratio increases at every radial station except for the blade tip,

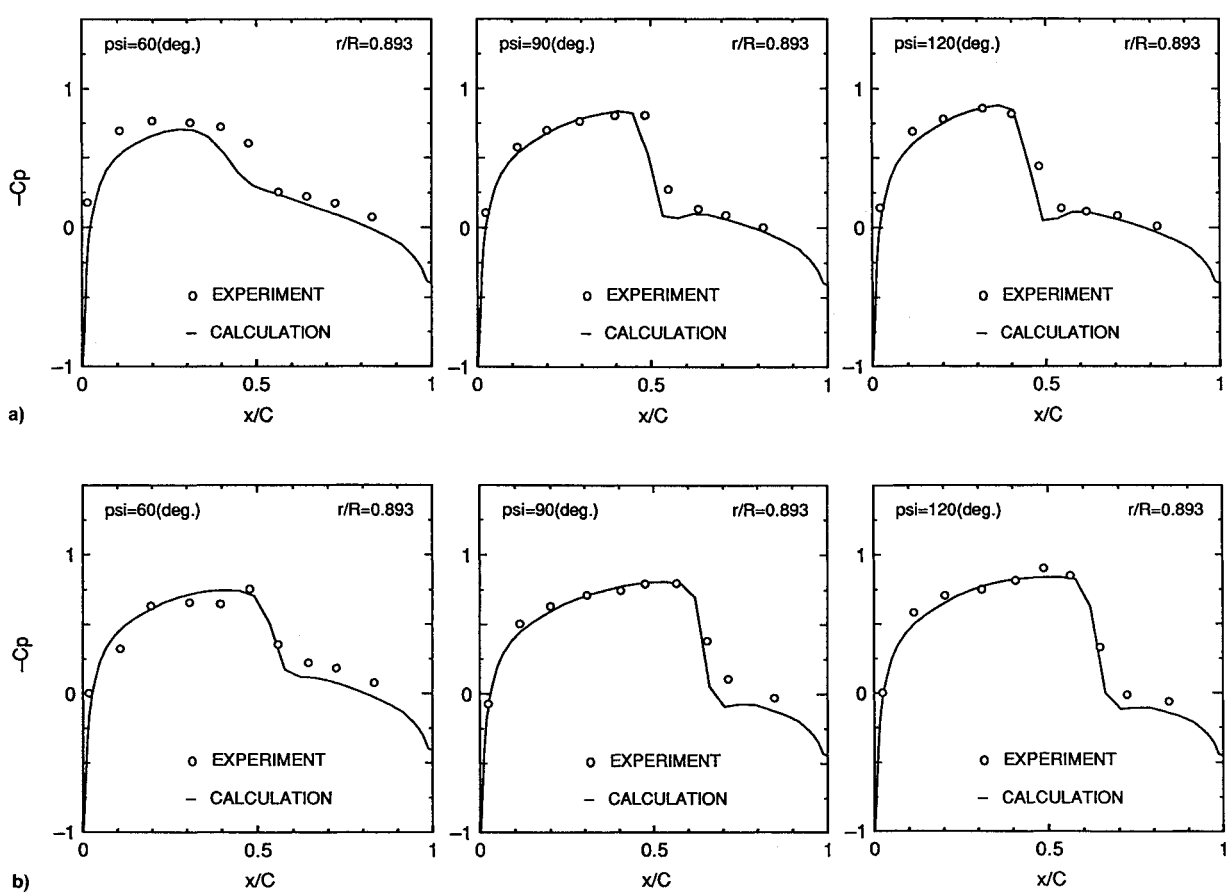

Fig. 1 Surface pressure distributions in nonlifting forward flight; AR = 7, NACA 0012, untwisted: a) $M_T = 0.7$, $\mu = 0.3$ and b) $M_T = 0.8$, $\mu = 0.2$.

as shown in Fig. 5a. At $\psi = 60$ deg, the shock wave becomes slightly stronger as the advance ratio decreases because M_n becomes larger as the advance ratio decreases at the outer radial station where the shock wave appears, as shown in Fig. 5b. At $\psi = 120$ deg, the shock wave becomes much stronger as the advance ratio increases, although the spanwise variation of M_n at $\psi = 120$ deg is the same as at $\psi = 60$ deg.

Effect of Sweep and Taper

Effect of Sweep

Figure 6a shows the spanwise variations of $\Delta(-C_p)$ for the blades with the swept-back tip planforms. The calculations are performed in the condition $M_T = 0.7$ and $\mu = 0.3$. The calculated planforms are illustrated in Fig. 6a. The initiation position of the swept-back tip is varied for each blade, and every blade has the same sweepback angle of 20 deg. The geometry of these blades is the same as the rectangular one except for the sweepback. A comparison of Fig. 6a with Fig. 4b shows that the swept-back tip planforms, except for the planform with the sweepback from $0.95R$, shift the peak position of $\Delta(-C_p)$ toward the outer radius region. It is also observed that the swept-back tip planforms, except for the planform with the sweepback from $0.95R$, decrease the peak value of $\Delta(-C_p)$ in the first quadrant, $0 \leq \psi \leq 90$ deg, and increase it in the second quadrant, $90 \leq \psi \leq 180$ deg. This is because the swept-back tip planforms delay the generation and growth of the shock wave. The difference in the behavior of the shock wave, however, is not large among these three planforms. Therefore, the planform with the sweepback from $0.90R$ is the best of the three because the increase of the torsional moment would be least in lifting condition. The effect of the sweepback on the shock-wave behavior in the planform with the sweepback from $0.95R$ is not as clear as in the other swept-back tip planforms because the peak of $\Delta(-C_p)$ for the rectangular tip planform appears at the radial station toward the inner radius from $0.95R$.

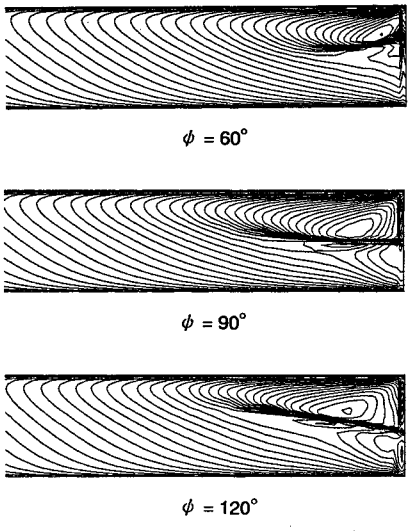

Fig. 2 Mach contours on blade surface; $M_T = 0.7$, $\mu = 0.3$, nonlifting.

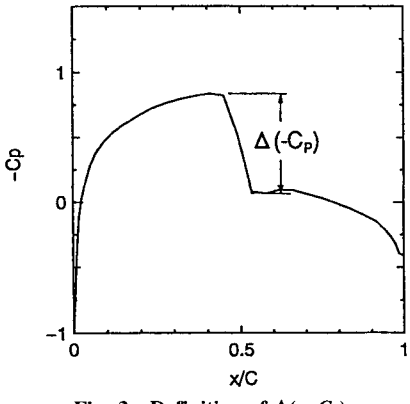

Fig. 3 Definition of $\Delta(-C_p)$.

The results of the calculations for the tip planforms with the sweepback angle of 40 deg are shown in Fig. 6b. A comparison of Fig. 6b with Fig. 4b shows that the large sweepback prevents the generation of strong shock waves, although it would cause an increase of the torsional moment in lifting condition. The swept-back tip planforms, except for the planform with the sweepback from $0.95R$, almost extinguish the shock wave at $\psi = 90$ deg and reduce the shock wave in the narrow region near the blade tip. The behavior of the shock wave in the planform with the sweepback from $0.95R$ shows a different tendency from the other swept-back planforms because of the reason mentioned previously, but this planform also prevents the generation of strong shock waves even though the modification from the rectangular tip planform is small.

Effect of Taper

The tapered tip planform has been used for good hover performance. The effect of the taper of the blade tip on the shock wave, which unsteadily occurs on the advancing side of a helicopter rotor, is investigated in detail.

Figure 7 shows the spanwise variations of $\Delta(-C_p)$ for the blades with the tapered tip planforms. The calculations are performed in the condition of $M_T = 0.7$, $\mu = 0.3$. Every blade has an NACA 0012 airfoil section along the entire blade span, even in the tapered region. Therefore, the thickness at the tapered region is smaller than that of the rectangular blade. A comparison of Fig. 7 with Fig. 4b shows that the tapered-tip planforms shift the peak position of $\Delta(-C_p)$ to-

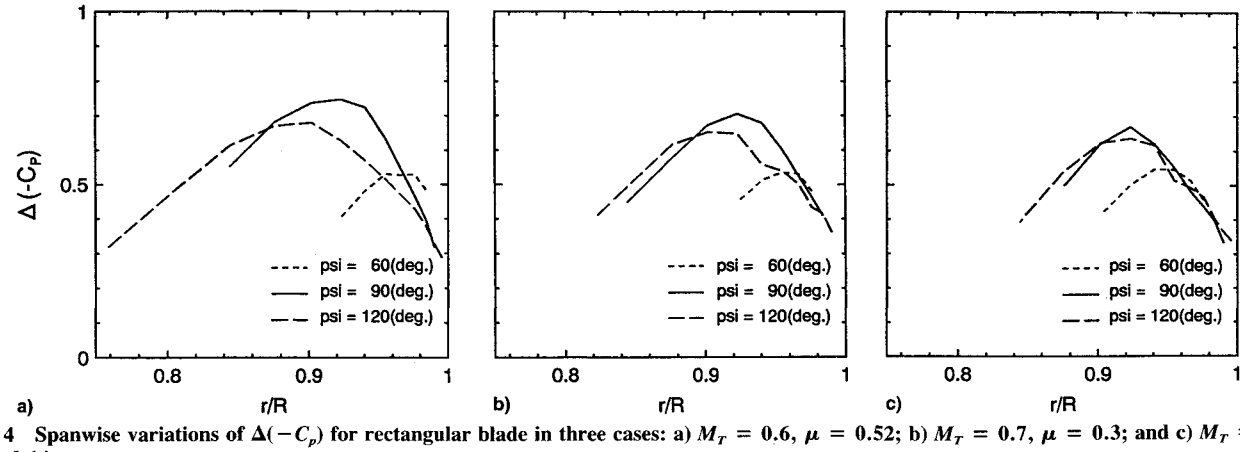

Fig. 4 Spanwise variations of $\Delta(-C_p)$ for rectangular blade in three cases: a) $M_T = 0.6$, $\mu = 0.52$; b) $M_T = 0.7$, $\mu = 0.3$; and c) $M_T = 0.8$, $\mu = 0.14$.

ward the outer radius region and increase the peak value of $\Delta(-C_p)$ in every azimuth position. This is caused by tip relief effect of the tip region, which will be explained in the next subsection. The tapered tip should not be used to weaken the shock wave.

Calculations are also performed for the tip planforms with the opposite taper, i.e., a taper ratio larger than 1.0. The results are shown in Fig. 8. A comparison of Fig. 8 with Fig. 4b shows that the opposite-tapered tip planforms shift the peak position of $\Delta(-C_p)$ toward the inner radius region and decrease the peak value of $\Delta(-C_p)$ in every azimuth position. This is also caused by the tip relief effect.

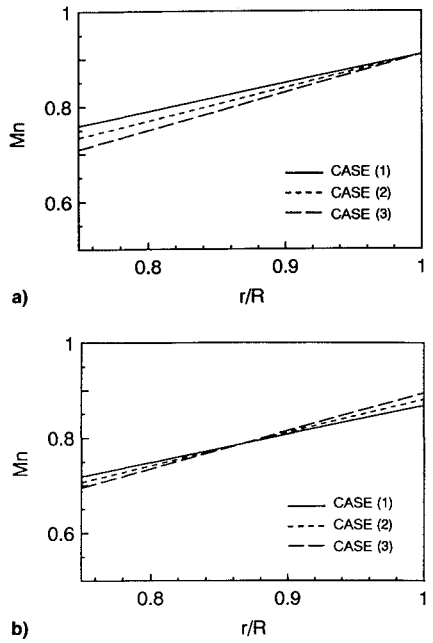

Fig. 5 Spanwise variations of M_n in three cases: a) ψ = 90 and b) ψ = 60 and 120 deg.

Tip Relief Effect

In order to explain the tip relief effect, calculations are performed for two kinds of blades in the nonrotational condition of $M_\infty = 0.9$, $M_T = 0.0$. These blades have the same radius and the same airfoil section, NACA 0012, but one blade has an AR of 10 and the other has 20. Figure 9a shows the Mach contours of the blade surfaces. The shock wave disappeared at the blade-tip region because of the spanwise flow. This phenomenon is known as the tip relief effect. Figure 9b shows the comparisons of the surface pressure distributions at the three different radial stations indicated in Fig. 9a. As shown in this figure, the surface pressure distributions of the two blades are similar to each other at the stations where the distances from the blade tip, which are nondimensionalized by the chord length, are the same. This indicates that the pressure distribution near a wingtip, the tip relief effect, is almost entirely determined by the nondimensionalized distance from the blade tip alone, and is less affected by the blade AR.

In order to explain the competition between the tip relief effect and the linearly increasing Mach number along the rotating blade, calculations are performed in the nonlifting forward flight condition of $M_T = 0.7$, $\mu = 0.3$. Figure 10 shows the effect of the AR on the surface pressure distributions at $0.95R$. The comparisons are shown at three azimuth positions in this figure. It is observed that the smaller AR blade, i.e., the larger chord length blade, decreases the strength of the shock wave and shifts its position toward the leading edge, although such a blade is thicker.

Trial of Blade Planform Design

The strong shock wave appears around $0.9R$ of a rectangular blade in the condition of $M_T = 0.7$, $\mu = 0.3$ as shown in Fig. 4b, and the shock wave is limited near the tip region alone. Therefore, the increase of the chord length near the tip region, such as the tip planform shown in Fig. 11a, may effectively restrict the shock wave using the tip relief effect. This planform is designed under a policy that the leading-edge position of a blade element is varied so that the chord

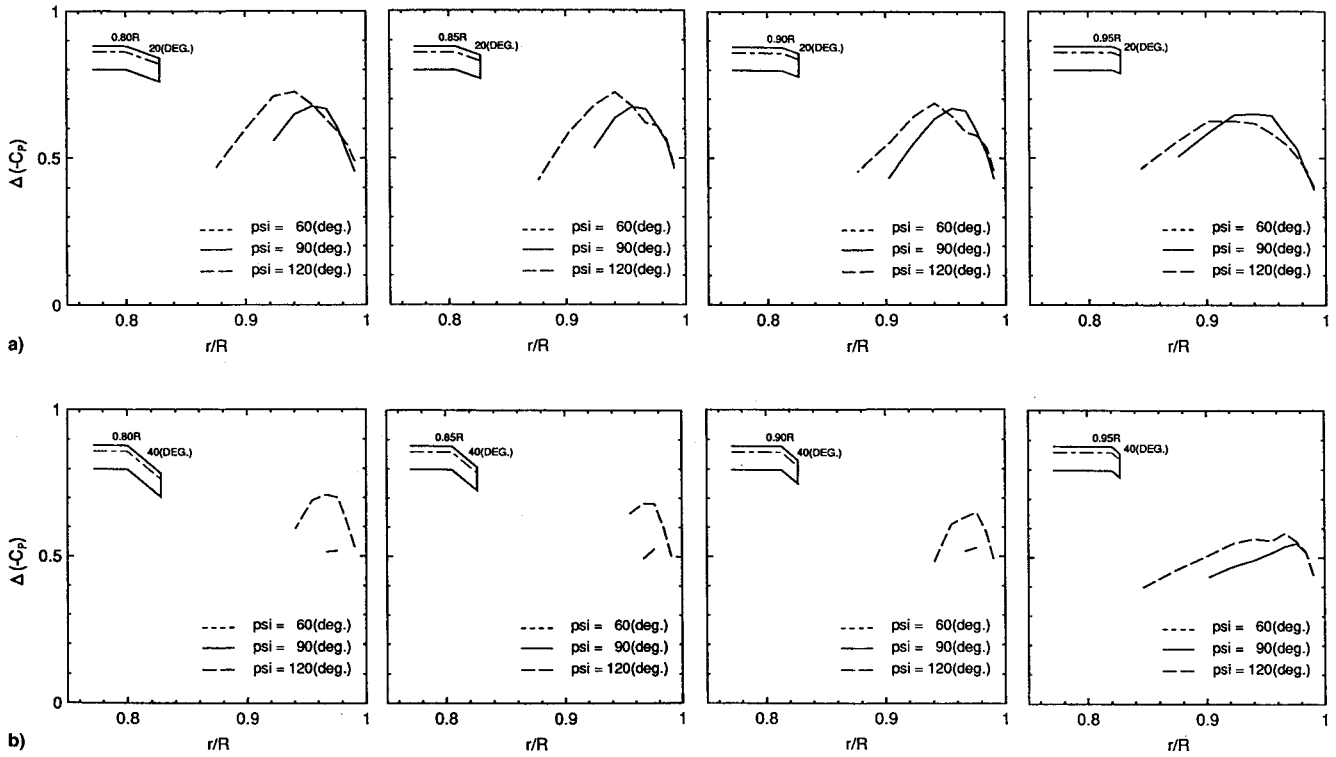

Fig. 6 Spanwise variations of $\Delta(-C_p)$ for swept-back tip blades; $M_T = 0.7$, $\mu = 0.3$, nonlifting: a) sweepback = 20 and b) 40 deg.

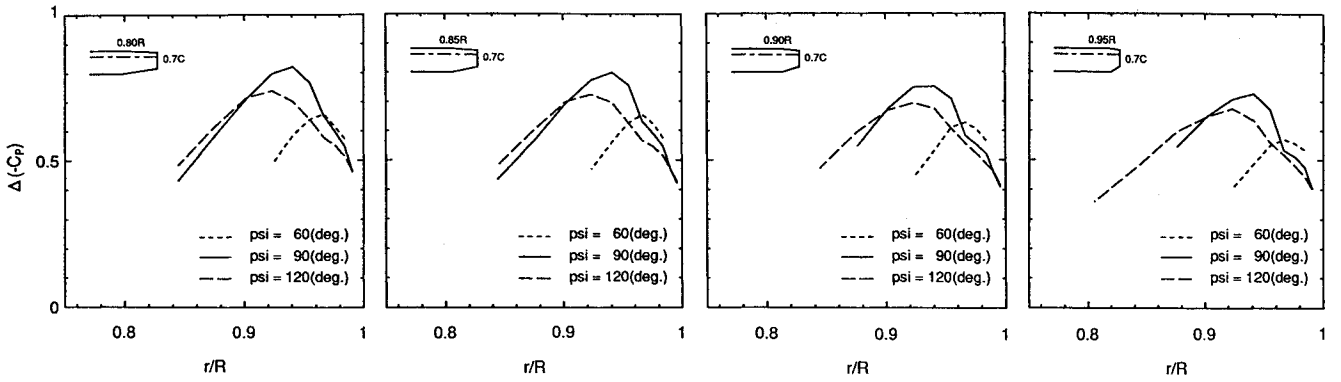

Fig. 7 Spanwise variations of $\Delta(-C_p)$ for tapered tip blades; $M_T = 0.7$, $\mu = 0.3$, nonlifting.

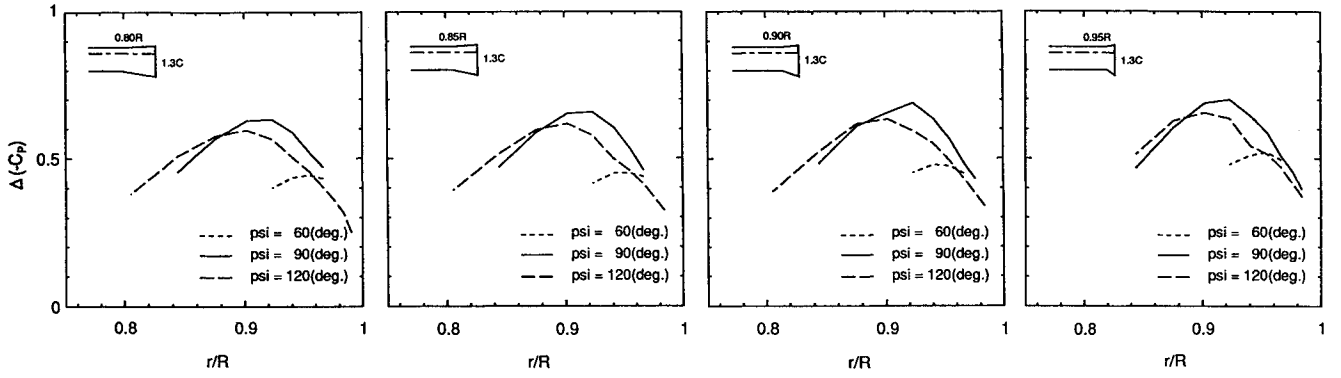

Fig. 8 Spanwise variations of $\Delta(-C_p)$ for opposite tapered tip blades; $M_T = 0.7$, $\mu = 0.3$, nonlifting.

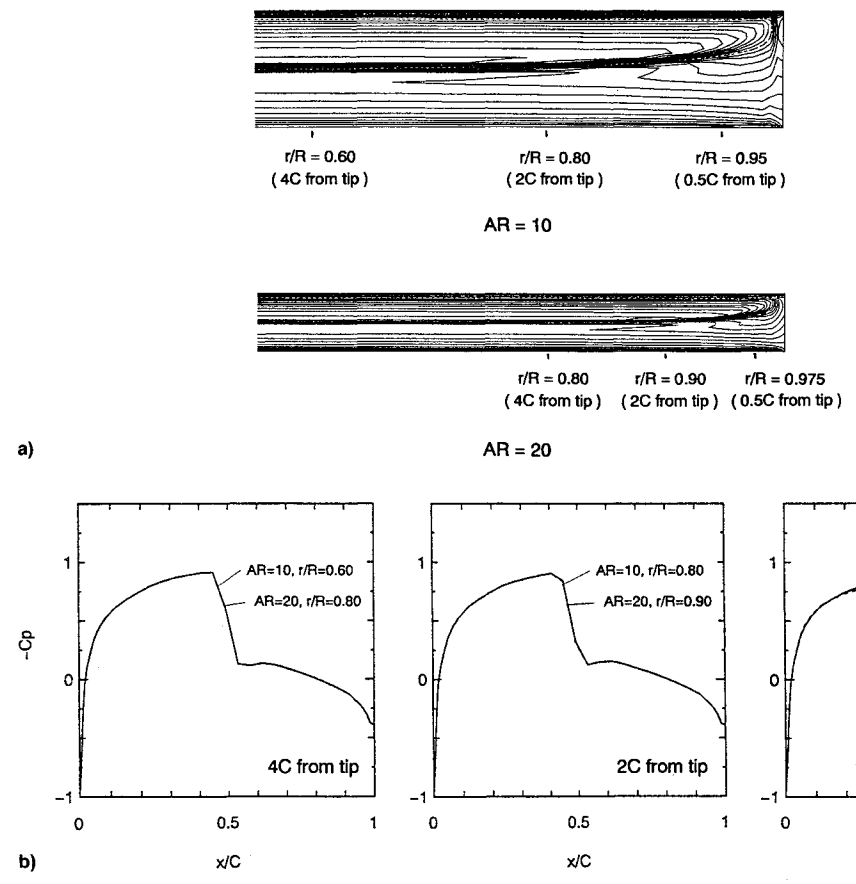

Fig. 9 a) Mach contours of nonrotational blade surfaces: $M_\infty = 0.9$, $M_T = 0.0$, NACA 0012 and b) comparisons of surface pressure distributions.

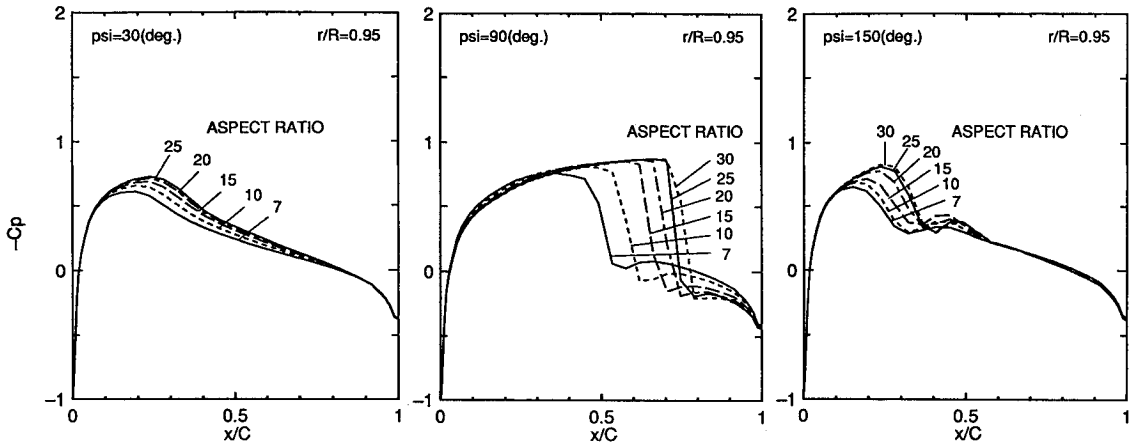

Fig. 10 Effect of AR on surface pressure distributions in nonlifting forward flight condition; $M_T = 0.7$, $\mu = 0.3$, NACA 0012.

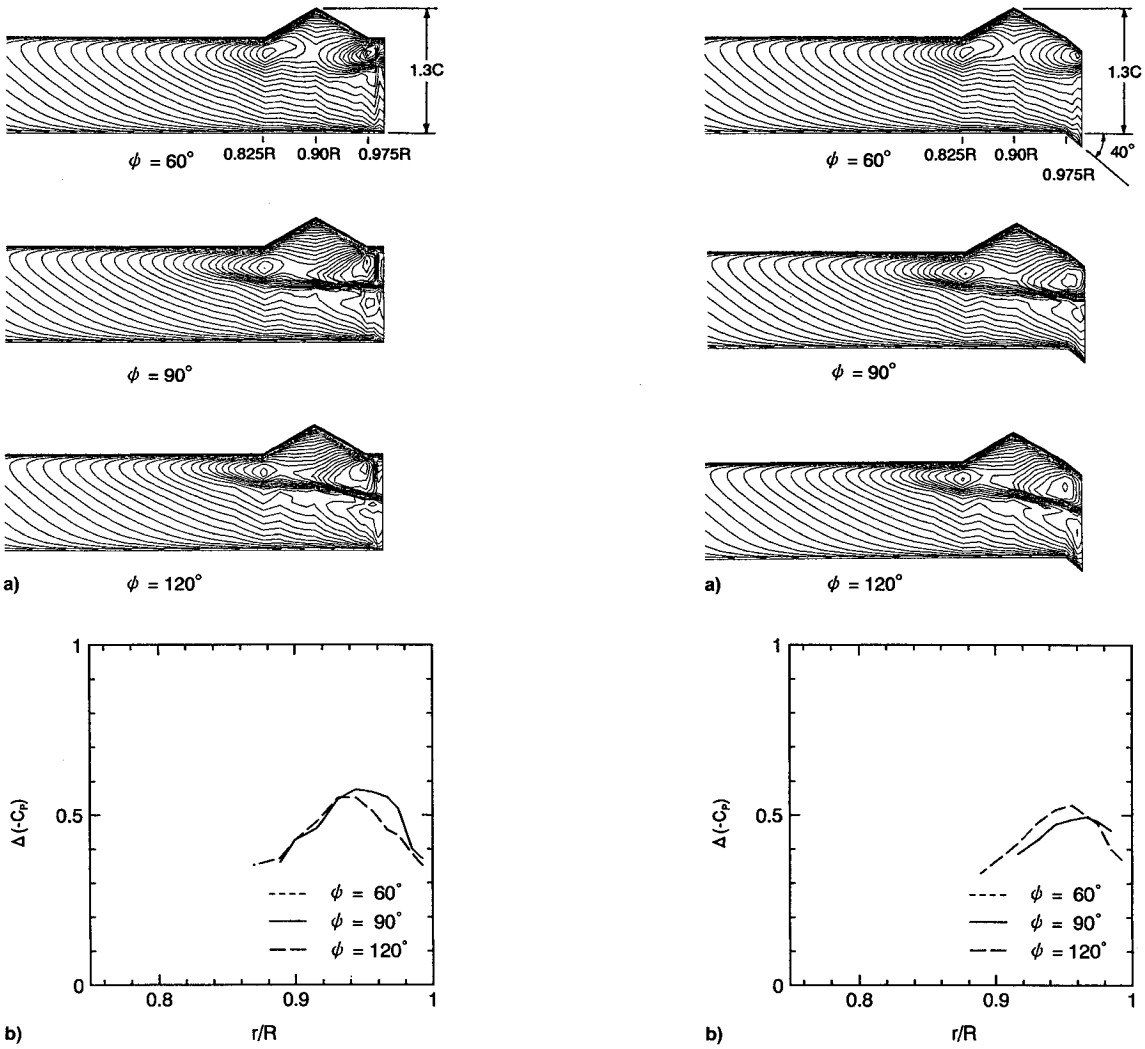

Fig. 11 a) Mach contours of blade with delta-shape extension of leading edge; $M_T = 0.7$, $\mu = 0.3$, NACA 0012 and b) spanwise variations of $\Delta(-C_p)$ for blade with delta-shape extension of leading edge; $M_T = 0.7$, $\mu = 0.3$, NACA 0012.

Fig. 12 a) Mach contours of blade with sweepback and delta-shape extension of leading edge; $M_T = 0.7$, $\mu = 0.3$, NACA 0012 and b) spanwise variations of $\Delta(-C_p)$ for blade with sweepback and delta-shape extension of leading edge; $M_T = 0.7$, $\mu = 0.3$, NACA 0012.

length is almost proportional to the shock-wave strength of the rectangular planform. The resultant planform is the delta-shape extension of the leading edge near the tip. The calculated Mach contours and the spanwise variations of the shock-wave strength are shown in Figs. 11a and 11b, respectively. A comparison of Fig. 11b with Fig. 4b shows that this planform limits the shock wave effectively, although the actual blade thickness is larger than that of the rectangular blade.

Another planform, which is designed based on the principle that the sweepback effect near the blade tip is combined with the tip relief effect, is indicated in Fig. 12a. The effectiveness of the swept-back planform near the blade tip was already demonstrated in Fig. 6b. The calculated Mach contours and the spanwise variations of the shock-wave strength are shown in Figs. 12a and 12b, respectively. A comparison of Fig. 12b with Fig. 11b shows that this planform limits the shock wave

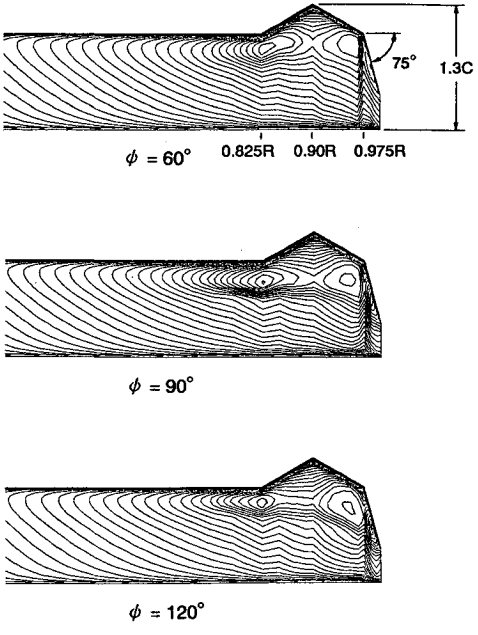

Fig. 13 Mach contours of blade with large sweepback and delta-shape extension of leading edge; $M_T = 0.7$, $\mu = 0.3$, NACA 0012.

more effectively than the delta-shape extension of the leading edge alone.

The larger sweepback of the leading edge is also examined and the resultant planform is indicated in Fig. 13. The shock wave is perfectly extinguished with this planform, and therefore, the figure of the spanwise variation of $\Delta(-C_p)$ is omitted. Although a shockless blade does not always improve the performance of a helicopter, it is important to restrict the shock-wave generation to avoid drag divergence.

Conclusions

The planform effect on the pressure distribution of a helicopter blade was analytically studied using the unsteady solution of Euler equations obtained by the CFD method. This study was focused on clarifying the shock-wave behavior on the blade tip on the advancing side. The following conclusions were reached based on the results of the present study.

1) The quantitative timewise variation of the shock-wave strength on the advancing blade of a helicopter rotor was presented in detail.

2) The effect of the sweep and taper of a blade-tip region on the behavior of the shock wave was presented.

3) A guideline for blade planform design on the advancing side is obtained and a newly devised tip planform that prevents shock-wave generation is indicated.

References

[1]Grant, J., "The Prediction of Supercritical Pressure Distributions on Blade Tips of Arbitrary Shape over a Range of Advancing Blade Azimuth Angles," *Vertica*, Vol. 3, 1979, pp. 275–292.

[2]Chattot, J. J., "Calculation of Three-Dimensional Unsteady Transonic Flows Past Helicopter Blades," NASA TP-1721, Oct. 1980.

[3]Arieli, R., Tauber, M. E., Saunders, D. A., and Caughey, D. A., "Computation of Transonic Flow About Helicopter Rotor Blades," *AIAA Journal*, Vol. 24, No. 5, 1986, pp. 722–727.

[4]Scott, M., Sigl, D., and Strawn, R., "Computational and Experimental Evaluation of Helicopter Rotor Tips for High Speed Forward Flight," AIAA Paper 89-1845, June 1989.

[5]Chang, I. C., and Tung, C., "Euler Solution of the Transonic Flow for a Helicopter Rotor," AIAA Paper 87-0523, Jan. 1987.

[6]Aoyama, T., Saito, S., and Kawachi, K., "Navier-Stokes Analysis of Blade Tip Shape in Hover," *Proceedings of the 16th European Rotorcraft Forum* (Glasgow, Scotland, UK), 1990, pp. I.4.1.1–I.4.1.12.

[7]Srinivasan, G. R., Raghavan, V., Duque, E. P. N., and McCroskey, W. J., "Flowfield Analysis of Modern Helicopter Rotors in Hover by Navier-Stokes Method," *Journal of the American Helicopter Society*, Vol. 38, No. 3, 1993, pp. 3–13.

[8]Aoyama, T., Kawachi, K., and Saito, S., "Unsteady Calculation for Flowfield of Helicopter Rotor with Various Tip Shapes," *Proceedings of the 18th European Rotorcraft Forum* (Avignon, France), 1992, pp. B03.1–B03.12.

[9]Caradonna, F. X., Laub, G. H., and Tung, C., "An Experimental Investigation of the Parallel Blade-Vortex Interaction," *Proceedings of the 10th European Rotorcraft Forum* (The Hague, The Netherlands), Paper 4, 1984, pp. 4.1–4.30.